Spin-lattice coupling induced phase transition in the $S=2$ frustrated antiferromagnet $CuMnO_2$

F. Damay,[1,*] M. Poienar,[2] C. Martin,[2] A. Maignan,[2] J. Rodriguez-Carvajal,[3] G. André,[1] and J. P. Doumerc[4]
[1]*Laboratoire Léon Brillouin, CEA-CNRS, UMR 12, CEA-Saclay, 91191 Gif-sur-Yvette Cedex, France*
[2]*Laboratoire CRISMAT, ENSICAEN, UMR 6508 CNRS, 6 Boulevard du Maréchal Juin, 14050 Caen Cedex, France*
[3]*Institut Laue-Langevin, 6 rue Jules Horowitz, BP 156, 38042 Grenoble Cedex 9, France*
[4]*Institut de Chimie de la Matière Condensée de Bordeaux, CNRS, Université de Bordeaux I, 87 Avenue du Dr. A. Schweitzer, 33608 Pessac Cedex, France*

(Received 8 April 2009; published 18 September 2009)

The crystal and magnetic structures of the layered oxide crednerite $CuMnO_2$ have been studied by neutron powder diffraction. In this system, which is topologically representative of a frustrated square lattice with nearest (J_1) and diagonal next-nearest- (J_2) neighbor interactions, three-dimensional antiferromagnetic ordering is observed below $T_N=65$ K, with propagation vector $\mathbf{k}_1=(-\frac{1}{2}\frac{1}{2}\frac{1}{2})$. Frustration is relieved through a strong magnetoelastic coupling to the lattice, evidenced by a structural phase transition from a monoclinic ($C2/m$) to a strained triclinic $C\bar{1}$ phase as magnetic order sets in. The magnetic order observed, which is described as spins antiferromagnetically aligned along [1-1 0] and ferromagnetically aligned along [1 1 0], corresponds to the so-called collinear antiferromagnetic order predicted for a frustrated two-dimensional antiferromagnetic Heisenberg model on a square lattice for $J_2/J_1>0.5$ in the presence of spin-lattice coupling.

DOI: 10.1103/PhysRevB.80.094410 PACS number(s): 61.05.fm, 75.25.+z, 75.30.Kz

I. INTRODUCTION

The role of frustrating interactions in low-dimensional systems is a crucial aspect of the physics of magnetism in condensed matter nowadays. Among strongly frustrated systems, the Heisenberg square lattice with nearest (J_1) and next-nearest- (J_2) neighbor interactions has been extensively studied in the framework of the connection between antiferromagnetism and copper-oxide superconductivity (see, for example, Ref. 1, and references within). It has been shown in particular that the introduction of frustration on such a lattice can lead to a Peierls-type transition from a tetragonal to an orthorhombic symmetry when spins are coupled to phonons: the rotational symmetry of the square lattice is broken as ferromagnetic and antiferromagnetic bonds acquire different lengths.[2,3] Indeed, on general grounds, the magnetic exchange coupling depends on the orbital overlap between atoms, overlap which changes with the actual distance between ions. Experimental evidences of this scenario are scarce so far;[4] topologically, however, the two-dimensional (2D) square lattice can also be considered as equivalent to the anisotropic triangular lattice with two in-plane magnetic exchange interactions, J_1 along two of the triangle directions and J_2 along the third one $(J_1 \neq J_2, (J_1, J_2)<0)$.[5] In this framework, delafossite oxides (general formula AMO_2, A being a monovalent cation in dumbbell coordination and M a transition metal) are interesting candidates, as their structure can be described as weakly coupled CdI_2-type layers of magnetic ions M with a triangular topology. The "standard" delafossite crystal structure is rhombohedral ($R\bar{3}m$) such as in $CuCrO_2$ or $CuFeO_2$,[6] and the magnetic lattice is a stacking of perfect triangular arrays. Though related to the delafossite structure, crednerite $CuMnO_2$ (Ref. 7) is not rhombohedral at room temperature (RT): in $CuMnO_2$, the Jahn-Teller (JT) distortion of the $Mn^{+3}(t_{2g}{}^3e_g^1)$ cation lifts the e_g orbitals degeneracy, thus leading to a distorted monoclinic structure, $C2/m$, at RT (Refs. 7 and 8) [Fig. 1(a)]. There is therefore in $CuMnO_2$ a large difference between apical and equatorial Mn-O distances within the MnO_6 octahedron; as a consequence, the resulting Mn^{+3} triangular sublattice is not regular but anisotropic, a topology equivalent to the frustrated square lattice with $J_2/J_1>1$ [Figs. 1(b) and 1(c)].

Very little is known about the low-temperature magnetic structure of crednerite $CuMnO_2$, even though its room-temperature crystal structure and antiferromagnetic properties have been known for a long time.[7,9] We report here a neutron diffraction investigation versus temperature of the crystal and magnetic structures of $CuMnO_2$. Around 80K, low-dimensionality magnetic scattering is observed, followed by three-dimensional magnetic ordering at $T_N=65$ K, characterized by the propagation vector $\mathbf{k}_1=(-\frac{1}{2}\frac{1}{2}\frac{1}{2})$. The rotational degeneracy of the ground state is lifted through magnetoelastic coupling, as evidenced by a lattice distortion resulting in a structural transition from a monoclinic to a triclinic phase at T_N. As predicted theoretically, the magnetic configuration is collinear type [C in Fig. 1(c)], and involves within the (a,b) plane ferromagnetic [1 1 0] chains, arranged antiferromagnetically along b and [1-1 0]. Chains coupling along c is antiferromagnetic.

II. EXPERIMENTAL SECTION

1 g of $CuMnO_2$ was prepared by high-temperature solid-state reaction. Stoichiometric amounts of CuO and MnO powders were weighed, carefully crushed together, and pressed in the form of bars, which were then put inside a platinum crucible, introduced in an evacuated ampoule, and heated up to 950 °C for 12 h. The quality of the compound was checked by x-ray diffraction, which confirmed that the sample is single phase, well crystallized, and exhibits the expected crednerite structure at room temperature. Magnetic susceptibility versus temperature was measured in 0.3 T, while warming from 1.5 to 300 K, after zero field cooling or field cooling, using a quantum design superconducting quan-

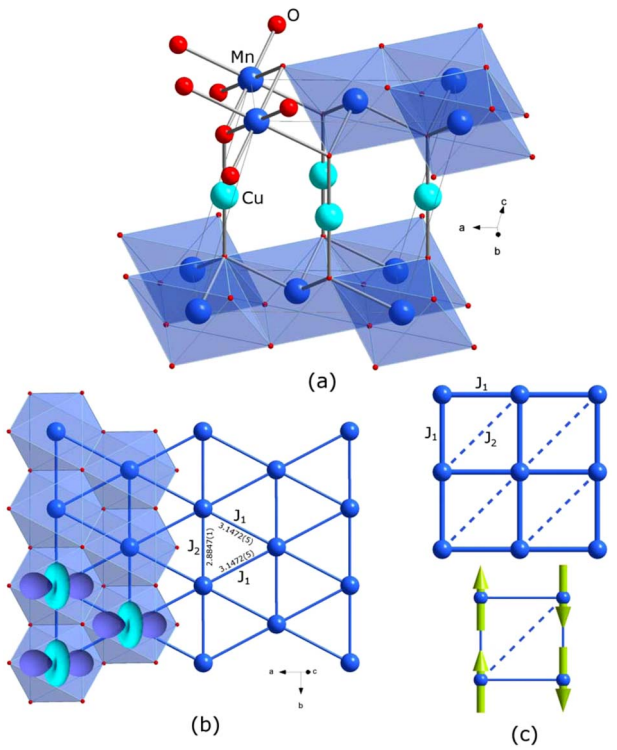

FIG. 1. (Color online) (a) Perspective view of the crednerite structure and (b) projection of the structure in the (a,b) plane evidencing the anisotropic triangular lattice with direct Mn-Mn exchange interactions J_1 and J_2 along $\langle 110 \rangle$ and b, respectively, (the specified Mn-Mn distances are those of the 300 K structure). MnO_6 octahedra are also represented along with d_{z^2} orbitals. (c) Topological equivalence with the square lattice with next (J_1) and next-nearest- (J_2) neighbor interactions. The collinear magnetic order is illustrated below.

tum interference device (SQUID) magnetometer: the observed temperature evolution of the susceptibility of our $CuMnO_2$ sample is similar to previous measurements by Doumerc *et al.*[9] Neutron powder diffraction (NPD) versus temperature was performed on the G4.1 diffractometer ($\lambda = 2.423$ Å) from 1.5 to 280 K, and high-resolution neutron diffractograms were recorded on the diffractometer 3T2 ($\lambda = 1.225$ Å) at 300 and 10 K. Both diffractometers are located at LLB, CEA-Saclay, France. Rietveld refinements of the powder diffractograms were performed with the FULLPROF program from the fullprof suite.[10]

TABLE I. Rietveld refinement results of the high-resolution neutron powder diffractogram of crednerite $CuMnO_2$ at 300 K. Cu and Mn cations occupy sites $2d$ $(0\frac{1}{2}\frac{1}{2})$ and $2a$ (0 0 0), respectively.

Space group	$C2/m$ ($n°12$)
Cell parameters	
a (Å)	5.5945(2)
b (Å)	2.8847(1)
c (Å)	5.8935(2)
β (deg)	103.97(2)
Cell volume (Å^3)	92.3(1)
Atomic positions	
O($4i$) x	0.4070(6)
y	0
z	0.1789(5)
Agreement factors	
R_{Bragg} (%)	0.88
χ^2	1.98

TABLE II. Anisotropic displacement factors in $CuMnO_2$ at 300 K($\times 10^4$) (from high-resolution NPD data).

	β_{11}	β_{22}	β_{33}	β_{13}
Cu	110(2)	236(5)	21(1)	8(1)
Mn	46(2)	85(8)	27(2)	12(2)
O	51(2)	112(4)	24(1)	10(1)

III. RESULTS AND DISCUSSION

A. Room-temperature crystal structure

The refinement of the RT high-resolution NPD data of $CuMnO_2$ (summarized in Table I) confirms earlier single-crystal x-ray diffraction results: $CuMnO_2$ crystallizes in a monoclinic $C2/m$ structure, with $a=5.5945(2)$ Å, $b=2.8847(1)$ Å, $c=5.8935(2)$ Å, and $\beta=103.97(2)°$. The Cu^+ and Mn^{+3} ions occupy the $2d$ $(0\frac{1}{2}\frac{1}{2})$and $2a$ (0 0 0) sites, respectively, and the oxygen atoms occupy the $4i$ position (x 0 y). As illustrated on Fig. 1(a), the crednerite structure can be described as layers in the (a,b) plane of edge-sharing MnO_6 octahedra, linked by Cu^+ ions linearly coordinated to two oxygen ions, thus forming O-Cu-O dumbbells perpendicular to the (a,b) plane, as in the delafossite structure. Anisotropic displacement factors and relevant structural distances and angles are reported in Tables II and III, respectively. β_{11} and β_{22} define displacements along a and b, respectively, and β_{33} corresponds to displacements parallel to

TABLE III. Selected interatomic distances (Å) (multiplicity in brackets) and angles (°) in $CuMnO_2$ at 300 K (from high-resolution NPD data). Subscripts $_\perp$ and $_\parallel$ correspond to perpendicular and parallel to the equatorial plane of the MnO_6 octahedron, respectively.

Mn-$O_\parallel$	1.9305(4) (×4)
Mn-$O_\perp$	2.2666(4) (×2)
Mn-Mn	2.8847(1) (×1)
	3.1472(5) (×2)
Cu-O	1.8377(3) (×2)
$[MnO_2]_\infty$ layer thickness	2.0458(3)
Mn-O-Mn	96.68(7)
	96.83(6)
$O_\parallel$-Mn-$O_\parallel$	96.68(7)
	83.31(6)
$O_\perp$-Mn-$O_\parallel$	96.83(6)
	83.17(6)

TABLE IV. Selected strain parameters values in $CuMnO_2$ at 300 K (from high-resolution NPD data).

S_{220}	S_{202}	S_{022}	S_{121}	S_{301}
0.36(10)	0.84(05)	0.72(11)	0.75(15)	0.53(04)

the c axis. The values listed in Table II underline the strong anisotropy of the structure: Cu^+ has the largest β_{11} and $\beta_{22}(>\beta_{33})$, corresponding to a flattened ellipsoid along c. Such flattened ellipsoids are often encountered in twofold linear coordination, and are described as resulting from transverse "guitar string" vibration.[11] The manganese ions in their distorted octahedral environment have the smallest anisotropic displacements factors, in agreement with the fact that the MnO_6 octahedra layers are close compact. Like Cu^+, their displacement ellipsoids are slightly flattened along c. All in all, equivalent isotropic displacement values U do not exceed 10.2×10^{-3} Å^2 for copper, 4.9×10^{-3} Å^2 for manganese, and 5.4×10^{-3} Å^2 for oxygen at 300 K, it is therefore reasonable to assume accordingly that oxygen nonstoichiometry or ionic disorder are negligible. We also tested in the refinement the possibility of a substitution of copper on the manganese sublattice, taking advantage of the contrasting neutron scattering lengths of Cu and Mn, but our results systematically lead to the expected $CuMnO_2$ stoichiometry within experimental resolution. However, to improve the refinement of the high-resolution NPD data, anisotropic microstrain parameters had to be introduced in the model. In this formalism, the microstrain effect is considered as equivalent to a distribution of the cell parameters, and the Gaussian component of the Bragg peaks width is modeled as a function of hkl using a set of S_{hkl} parameters as fourth-term expansion.[12] This lead to slightly but clearly better agreement factors, and, accordingly, the strain parameter values remained small (Table IV): this microstrain is nevertheless indicative of a lattice parameter distribution defect, which we relate to the existence of a $Cu_{1+x}Mn_{1-x}O_2$ type solid solution[13] within the sample.

As expected for a JT active ion such as Mn^{+3}, the MnO_6 octahedra in $CuMnO_2$ are elongated. The longest Mn-O interatomic distances [Mn-O=2.2666(4) Å] correspond to the direction of the occupied d_{z^2} orbitals. Because these orbitals are all pointing in the same direction, this results in ferro-orbital ordering in the (a,c) plane. The d_{z^2} orbitals are perpendicular to the empty $d_{x^2-y^2}$ orbitals, which point toward the four closer oxygen atoms, with Mn-O=1.9305(4) Å. The resulting distorted triangular lattice formed by the Mn^{+3} ions is illustrated on Fig. 1(b). The triangles are formed by one short Mn-Mn distance of 2.8847(1) Å (corresponding to magnetic exchange J_2) and two longer Mn-Mn distances of 3.1472(5) Å (corresponding to J_1). In this edge-sharing octahedra configuration, superexchange interactions through a Mn-O-Mn path involve angles close to 90° (see Table III) and are consequently quite weak.[14] On the other hand, half-filled t_{2g} orbitals directed along the short Mn-Mn distance of edge-sharing octahedra should favor strong antiferromagnetic direct exchange between Mn^{+3} ions.[14] Magnetic interactions between $[MnO_2]_\infty$ layers are expected to be much weaker, since $(Mn\text{-}Mn)_{inter}$=5.8935(2) Å (the actual distance between magnetic $[Mn]_\infty$ planes is somewhat shorter, 5.7190(1) Å, because of the monoclinic distortion). Three-dimensional (3D) magnetic ordering is nonetheless observed below 65 K, as will be exposed in Sec. III C.

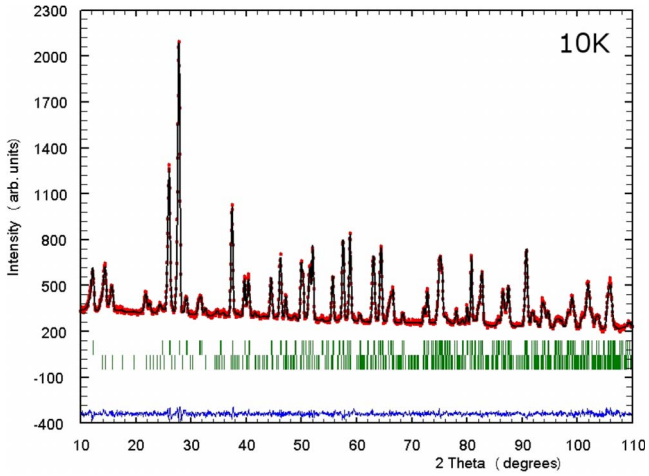

FIG. 2. (Color online) Refinement of the 10 K neutron diffraction data of $CuMnO_2$ recorded with the 3T2 diffractometer (λ =1.225 Å). Experimental data are represented by open circles, the calculated profile by a continuous line, and the allowed structural (upper row) and magnetic (lower row) Bragg reflections by vertical marks. The difference between the experimental and calculated profiles is displayed at the bottom of the graph.

B. Low-temperature crystal structure

The refinement of the high-resolution NPD data at 10 K shows that the structure cannot be described with a monoclinic space group like at room temperature, as the low Q Bragg reflections are slightly offset with respect to their calculated positions in the $C2/m$ space group. These offsets can be readily taken into account by a lowering of the crystal-structure symmetry using a "pseudomonoclinic" $C\bar{1}$ unit cell, which allows keeping the same unit cell as the $C2/m$ one. Without the binary axis, the three cell angles are now refinable parameters and the oxygen is in general position (x,y,z). In addition, a substantial anisotropic broadening of hkl Bragg peaks is also observed on the 10K neutron data, and is modeled in the refinement through the use of anisotropic microstrain parameters, as for the 300K data.

As illustrated on Fig. 2, this leads to a reasonably good refinement of the data, with R_{Bragg}=2.52% and χ^2=1.44 (these values are obtained taking into account in the refinement the magnetic structure that is described in Sec. III C). Results of the refinement are reported in details in Tables V–VII. At 10 K, the cell parameters of $CuMnO_2$ in the $C\bar{1}$ space group are a=5.5806(8) Å, b=2.8799(4) Å, c =5.8925(8) Å, α=90.18(2)°, β=103.98(1)° and γ =89.81(1)°. As expected, the values of the strain parameters (Table VII) show that anisotropic strain is much more pronounced at 10 K than at RT, as a consequence of the triclinic structural distortion.

TABLE V. Rietveld refinement results of the 3T2 and G4.1 neutron powder diffractograms of crednerite $CuMnO_2$ at 10 K. Cu and Mn cations occupy sites $2d$ $(0\frac{1}{2}\frac{1}{2})$ and $2a$ (0 0 0), respectively.

Space group	$C\bar{1}$ $(n°2)$
Cell parameters	
a (Å)	5.5806(8)
b (Å)	2.8799(4)
c (Å)	5.8925(8)
α (deg)	90.18(2)
β (deg)	103.98(1)
γ (deg)	89.81(1)
Cell volume (Å^3)	91.9(2)
Atomic positions	
O($4i$) x	0.4062(6)
y	–0.012(8)
z	0.1786(2)
Agreement factors	
R_{Bragg} (%)	2.52
χ^2	1.44
Mn magnetic moment (μ_B) ($\{\mathbf{k}_1\}$ structure, from G4.1 data)	
along a	2.94(3)
along c	1.76(6)
$R_{\text{Bragg magnetic}}$ (%)	4.32

Compared with the room-temperature structure, there is a clear decrease in the Mn-Mn distances building the triangular lattice: along b (which corresponds to the exchange interaction J_2), Mn-Mn decreases from 2.8847(1) to 2.8799(4) Å, which is equivalent to a ~0.17% contraction. In addition, the triclinic distortion at 10 K leads to two different shorter Mn-Mn distances, 3.1442(4) and 3.1357(4) Å along [1 1 0] and [1-1 0], respectively, to be compared with Mn-Mn=3.1472(5) Å at RT. A contraction of ~0.37% of the Mn-Mn interatomic distance occurs along [1-1 0], much stronger than the 0.09% Mn-Mn contraction observed along [1 1 0]. This will clearly have major consequences on the magnetic arrangement, as the frustration of the J_1 magnetic exchange is lifted by such a distortion, and will be further discussed below.

TABLE VI. Selected interatomic distances (Å) (multiplicity in brackets) and angles (°) in $CuMnO_2$ at 10K (from high-resolution NPD data).

Mn-$O_{\parallel}$	1.9352(19) (×2)
	1.9225(19) (×2)
Mn-$O_{\perp}$	2.2562(11) (×2)
Mn-Mn	2.8799(4) (×1)
	3.1442(4) (×1)
	3.1357(4) (×1)
Cu-O	1.8395(12) (×2)
$[MnO_2]_{\infty}$ layer thickness	2.0413(11)
Mn-O-Mn	96.58(10)
	96.92(5)
$O_{\parallel}$-Mn-$O_{\parallel}$	83.42(7)
	96.58(7)
$O_{\perp}$-Mn-$O_{\parallel}$	83.08(5)
	96.92(5)

TABLE VII. Selected strain parameters values in $CuMnO_2$ at 10 K (from high-resolution NPD data).

S_{220}	S_{202}	S_{022}	S_{121}	S_{301}
2.4(7)	4.9(3)	7.0(8)	8.0(13)	2.3(2)

There is also a relatively important shortening of the longest Mn-$O_{\perp}$ distance (subscript $_{\perp}$ corresponds to apical oxygen atoms within the MnO_6 octahedra), from 2.2666(4) Å at RT to 2.2562(11) Å at 10 K. As a consequence, the average Mn-O distance within an octahedron decreases at 10 K, and the MnO_6 octahedron is also slightly less distorted at 10 K than at RT. The Cu-O distance increases slightly as T decreases, whereas the $[MnO_2]_{\infty}$ layer thickness decreases, these two effects probably compensating each other explain the fact that c remains roughly constant with temperature.

C. Evolution with temperature of the crystal and magnetic structures

The temperature evolution between 300 and 1.5 K of the NPD patterns is illustrated on Fig. 3. Because of the medium instrumental resolution and narrow Q range of the G4.1 NPD data, the structural transition is only detectable through a very slight shift of the magnetic peak positions at the onset of the 3D magnetic ordering (~65 K on Fig. 3), and therefore all the G4.1 data crystal-structure refinements were performed in the $C2/m$ space group; it is clear however from the neutron data that the magnetic structure cell is triclinic, and that the monoclinic to triclinic transition is concomitant with the 3D magnetic ordering at 65 K, as further evidenced in the temperature evolution of the lattice parameters (Fig.

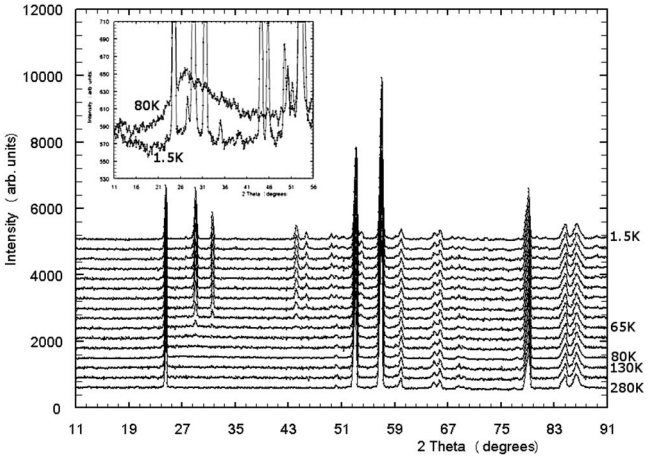

FIG. 3. Evolution between 1.5 and 280 K of the neutron diffractograms of $CuMnO_2$ (G4.1 diffractometer, λ=2.423 Å). Inset: comparison of the magnetic diffuse scattering signal around 1.23 Å^{-1} at 80 and 1.5 K.

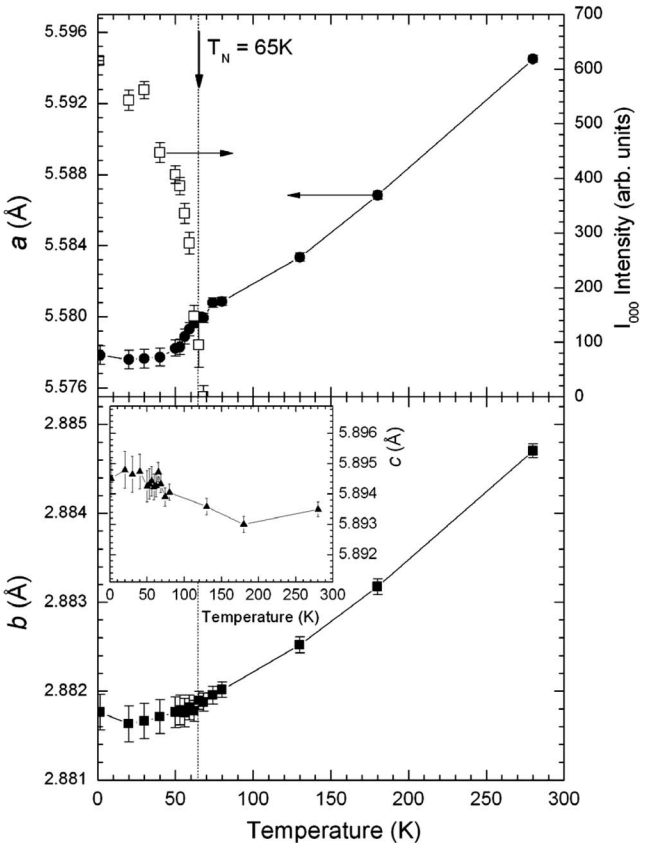

FIG. 4. Temperature evolution of the a and b lattice parameters (in the space group $C2/m$) of $CuMnO_2$, and evolution with temperature of the intensity of the magnetic Bragg peak I_{000} of the $\{\mathbf{k}_1\}$ structure. Inset: temperature dependence of lattice parameter c of $CuMnO_2$.

4). The cell parameters a, b, and c have very distinct behaviors with temperature: while parameter a (top panel of Fig. 4) exhibits a steady decrease followed by a sharp contraction around 65 K, b decreases steadily between 300 and 10 K, with no distinct accident at 65 K (bottom panel of Fig. 4). The c cell parameter (inset of Fig. 4) on the other hand hardly changes over the whole temperature range, within the experimental resolution, as already pointed out when comparing the 10 and 300 K structures. For $T \leq 40$ K, a, b, and c become roughly constant and correspond to the values obtained for the triclinic cell of $CuMnO_2$ at 10 K. It is noteworthy that the lattice distortion occurs within the (a,b) plane only, which corresponds to the anisotropy of the frustration.

With decreasing temperature, before 3D magnetic ordering, magnetic diffuse scattering becomes also clearly observable on the NPD data from 80 K downwards, around $Q = 1.23$ Å^{-1} ($2\theta \sim 27.5°$ in inset of Fig. 3). The magnetic diffuse scattering intensity increases until the appearance of magnetic Bragg peaks around 65 K. It is likely here, considering the strong 2D character of the structure of $CuMnO_2$, that magnetic ordering starts within planes, thus giving rise to a 2D-like magnetic scattering feature (although one-dimensional ordering along b could also be plausible here, since $J_1 < J_2$). Below 65 K, the diffuse scattering signal decreases, but is still noticeable at 1.5 K (inset of Fig. 3).

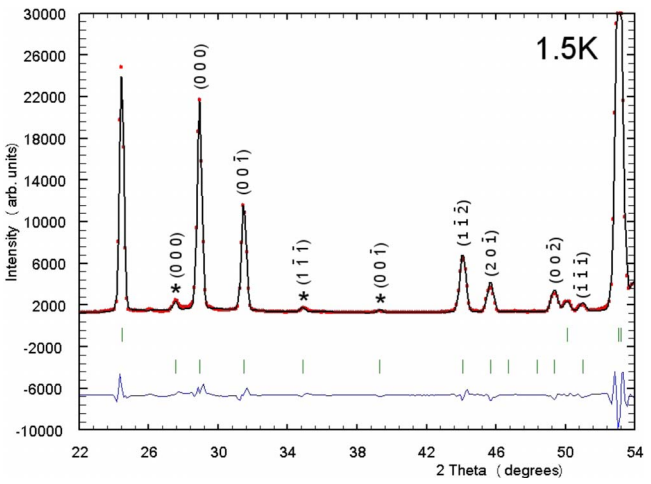

FIG. 5. (Color online) Enlargement of the refinement of the neutron diffraction data of $CuMnO_2$ at 1.5 K (using G4.1 diffractometer). Magnetic peaks indexation is shown for both propagation vectors $\mathbf{k}_1$ and $\mathbf{k}_2$ (magnetic peaks belonging to $\{\mathbf{k}_2\}$ are distinguished by the symbol *). Experimental data are represented by open circles, the calculated profile by a continuous line, and the allowed structural (upper row) and magnetic (lower row) Bragg reflections by vertical marks. The difference between the experimental and calculated profiles is displayed at the bottom of the graph.

As T reaches 65 K, magnetic Bragg peaks become apparent on the low-temperature NPD data. They can be divided into two families (Fig. 5): the first family, which corresponds to the largest magnetic peaks, can be indexed with the propagation vector $\mathbf{k}_1 = (-\frac{1}{2}\frac{1}{2}\frac{1}{2})$. The second family corresponds to magnetic peaks of much smaller intensity, and can be indexed with a propagation vector belonging to a different star, $\mathbf{k}_2 = (-\frac{1}{2}\frac{1}{2}0)$ [or $\mathbf{k}_2 = (\frac{1}{2}\frac{1}{2}0)$: it is actually not possible to differentiate unambiguously between these two propagation vectors, as the magnetic signal is very weak]. Within the temperature resolution, these two families of peaks appear simultaneously on the neutron diffractograms, and originate from the same diffuse scattering signal. According to results which will be reported elsewhere,[15] the $\{\mathbf{k}_2\}$ magnetic peaks can be attributed to the existence of a $Cu_{1+x}Mn_{1-x}O_2$ like composition distribution within the sample,[13] in agreement with the microstructural strain observed at RT.

The $\{\mathbf{k}_1\}$ spin configuration is rather straightforward (Fig. 6). It describes antiferromagnetic chains running along b; within the (a,b) plane, these chains are arranged antiferromagnetically along [1-10] and ferromagnetically along [1 1 0]. Adjacent (a,b) planes are coupled antiferromagnetically along c. $\mathbf{k}_2$ actually describes a similar antiferromagnetic arrangement in the (a,b) planes, but with the planes ferromagnetically coupled along c. Using these two propagation vectors, we can reproduce the data in a very satisfactory way (Fig. 5), with $R_{\text{Bragg}} = 1.6\%$ and magnetic $R_{\text{Bragg}} = 4.9\%$. At 1.5 K, the components of the magnetic moment for the $\mathbf{k}_1$ vector are 2.94(3) and 1.76(6)μ_B along the a and c axes of the $C\bar{1}$ cell, respectively, which corresponds to 3.05μ_B per Mn^{+3} cation. The spins actually point along the direction of

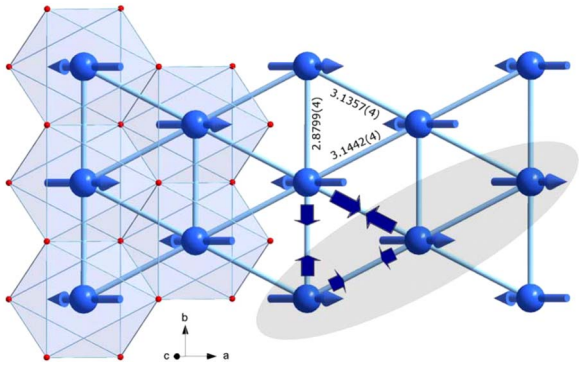

FIG. 6. (Color online) Illustration of the magnetic structure of $CuMnO_2$, corresponding to propagation vectors $\mathbf{k}_1=(-\frac{1}{2}\frac{1}{2}\frac{1}{2})$. Along c, magnetic coupling between layers is antiferromagnetic. A ferromagnetic chain along [1 1 0] is evidenced by the shaded area. The specified Mn-Mn distances are those of the 10 K triclinic structure, the large arrows illustrate accordingly the different degrees of contraction of the Mn-Mn triangular lattice with respect to the RT structure.

the d_{z^2} orbitals, as could be expected from the easy-axis anisotropy of the Mn^{+3} site. For the propagation vector $\mathbf{k}_2$, moments have components of $0.4(2)\mu_B$ along a and $-0.4(4)\mu_B$ along b. The standard deviations on these values are high, and the direction of the moment within the (a,b) plane is, as a result, rather hypothetic. $0.6\mu_B$ per Mn^{+3} can be refined for the $\mathbf{k}_2$ magnetic structure, the total magnetic moment per Mn^{+3} is therefore $3.65\mu_B$. It is indeed expected to be lower than the expected saturation value of $4\mu_B$ for Mn^{+3} in its high spin ($S=2$) configuration, because of the remaining diffuse magnetic scattering at 1.5 K.

D. Discussion

Among the possible lattice deformations that can be considered for the square lattice, three are stable, depending on the values of the exchange integrals J_1 and J_2 and on the spin-lattice coupling constants.[2] For $J_2/J_1>0.5$, even a weak coupling to the lattice is enough to stabilize the antiferromagnetic collinear phase and to induce a structural distortion to an orthorhombic lattice, with two different bond lengths in the x and y directions, corresponding to two different nearest-neighbor interactions. $CuMnO_2$ is a remarkable experimental realization of such a structural distortion upon magnetic ordering, and evidences the role of the spin-lattice coupling to lift the frustration in this compound. As magnetic moments order, the antiferromagnetic chains running along b are pushed closer to each other, as evidenced by the strong contraction of the a parameter. Antiparallel ordering of the spins along [1-1 0] chains leads to a large decrease (0.39% with respect to the RT value) of the corresponding Mn-Mn distance, while the Mn-Mn distance involved in the ferromagnetic arrangement along [1 1 0] only decreases by 0.09% compared to the RT value: this anisotropic contraction of the manganese triangular array releases the initial frustration of the J_1 magnetic exchange interaction. Since low-dimensionality magnetic scattering is also observed in this compound, it is possible that the lattice distortion and the breaking of the rotational symmetry actually start within planes before 3D magnetic ordering sets in.

A similar geometry of the Mn^{+3} sublattice is also observed in $NaMnO_2$,[16] for which magnetoelastic coupling and symmetry breaking phenomena have been reported not long ago.[17] In $NaMnO_2$, low dimensionality is much more predominant and coexists with the 3D antiferromagnetic ($T_N=45$ K) down to 4 K. Similar frustration lifting lattice distortions are observed in both compounds; the antiferromagnetic spin configuration characterized by a propagation vector $\mathbf{k}=(\frac{1}{2}\frac{1}{2}0)$ in $NaMnO_2$, is, in the (a,b) plane, identical (collinear-like) to that of $CuMnO_2$. The coupling between adjacent planes is, however, ferromagnetic in $NaMnO_2$. Na^+ ions are much larger than Cu^+ ions, but being in octahedral sites, the magnetic planes are actually closer to each other than in $CuMnO_2$. Linear Cu-O bonding promotes stronger antiferromagnetic superexchange than Na-O bonding: this leads in $CuMnO_2$ to a higher T_N and to antiferromagnetic coupling of the $[MnO_2]_\infty$ planes along c. Interplane coupling is, however, in either compound, not expected to play a role in the frustration lifting mechanism.

Our results evidence the different structural and magnetic responses to frustration of the M triangular lattice in the $CuMO_2$ system: in $CuCrO_2$, helicoidal antiferromagnetic ordering occurs below $T_N=24$ K on the Cr equilateral triangular lattice, and is concomitant with a relaxation of the CrO_6 octahedra,[18] but no lattice distortion is observed. In $CuFeO_2$,[19] a structural transition from rhombohedral to monoclinic $C2/m$ is observed at T_N, which results in a Fe isosceles triangle lattice with rotational symmetry enabling a commensurate antiferromagnetic ordering. Spin-lattice coupling also appears to be the key parameter to understand the magnetic structure of $CuMnO_2$, but a more theoretical approach would be required at this point to understand the underlying physical mechanisms responsible for the evolution with M of the transition-metal lattice symmetry below T_N.

IV. CONCLUSION

In conclusion, a neutron powder diffraction investigation of $CuMnO_2$ has shown that at $T_N=65$ K, long range 3D magnetic ordering occurs simultaneously with a lowering of the monoclinic symmetry to a triclinic one. The corresponding lattice distortion, which affects the symmetry and distances of the Mn sublattice within the (a,b) plane, results in the differentiation of the antiferromagnetic and ferromagnetic bond lengths below T_N. $CuMnO_2$ appears to be a good example of a quasi-two-dimensional frustrated antiferromagnet in which the magnetic phase transition is strengthened by spin-lattice coupling.

ACKNOWLEDGMENTS

The authors thank Stéphane Cueille, Carlo Vecchini, Alexandros Lappas, Sylvain Petit, and Laurent Chapon for fruitful discussions. Financial support for this work was partially provided by the French Agence Nationale de la Recherche under Grant No. ANR-08-BLAN-0005-01.

*francoise.damay@cea.fr

[1] P. Chandra, P. Coleman, and A. I. Larkin, Phys. Rev. Lett. **64**, 88 (1990).
[2] F. Becca and F. Mila, Phys. Rev. Lett. **89**, 037204 (2002).
[3] C. Weber, F. Becca, and F. Mila, Phys. Rev. B **72**, 024449 (2005).
[4] R. Melzi, P. Carretta, A. Lascialfari, M. Mambrini, M. Troyer, P. Millet, and F. Mila, Phys. Rev. Lett. **85**, 1318 (2000).
[5] Zheng Weihong, R. H. McKenzie, and R. P. Singh, Phys. Rev. B **59**, 14367 (1999).
[6] C. T. Prewitt, R. D. Shannon, and D. B. Rogers, Inorg. Chem. **10**, 719 (1971).
[7] I. D. Kondrashev, Sov. Phys. Crystallogr. **3**, 703 (1959).
[8] J. Topfer, M. Trari, P. Gravereau, J. P. Chaminade, and J. P. Doumerc, Z. Kristallogr. **210**, 184 (1995).
[9] J. P. Doumerc, M. Trari, J. Topfer, L. Fournes, J. C. Grenier, M. Pouchard, and P. Hagenmuller, Eur. J. Solid State Inorg. Chem. **31**, 705 (1994).
[10] J. Rodriguez-Carvajal, Physica B (Amsterdam) **192**, 55 (1993).
[11] J. S. O. Evans, J. Chem. Soc. Dalton Trans., **19**, 3317 (1999).
[12] J. Rodriguez-Carvajal, M. T. Fernandez-Diaz, and J. L. Martinez, J. Phys.: Condens. Matter **3**, 3215 (1991).
[13] M. Trari, J. Topfer, P. Dordor, J. C. Grenier, M. Pouchard, and J. P. Doumerc, J. Solid State Chem. **178**, 2751 (2005).
[14] J. B. Goodenough, Phys. Rev. **117**, 1442 (1960).
[15] M. Poienar *et al.* (unpublished).
[16] M. Jansen and R. Hoppe, Z. Anorg. Allg. Chem. **399**, 163 (1973).
[17] M. Giot, L. C. Chapon, J. Androulakis, M. A. Green, P. G. Radaelli, and A. Lappas, Phys. Rev. Lett. **99**, 247211 (2007).
[18] M. Poienar, F. Damay, C. Martin, V. Hardy, A. Maignan, and G. André, Phys. Rev. B **79**, 014412 (2009).
[19] F. Ye, Y. Ren, Q. Huang, J. A. Fernandez-Baca, P. Dai, J. W. Lynn, and T. Kimura, Phys. Rev. B **73**, 220404(R) (2006).